Structural and ultrastructural organization of the parietal cortex and dorsal hippocampus in transgenic 5xFAD mice administered sodium valproate, a histone deacetylase inhibitor

Natalia L. Tumanova,[1] Dmitrii S. Vasiliev,[1] Nadezhda M. Dubrovskaya,[1] Natalia N. Nalivaeva[2]

[1]I. M. Sechenov Institute of Evolutionary Physiology and Biochemistry, Russian Academy of Sciences, St. Petersburg, Russia; [2]School of Biomedical Sciences, Faculty of Biological Sciences, University of Leeds, United Kingdom

Correspondence: Dimitrii S. Vasiliev, I. M. Sechenov Institute of Evolutionary Physiology and Biochemistry, Russian Academy of Sciences, St. Petersburg, Russia.
E-mail: dvasilyev@bk.ru

Key words: 5xFAD transgenic mice, parietal cortex, dorsal hippocampus, neurodegeneration, amyloid peptide, sodium valproate, neprilysin, astroglia.

Contributions: NLT, microscopy, morphological studies, article writing; DSV, rtPCR and Western blot analyses, statistical data processing; NMD, experiments with animals, sodium valproate treatment; NNN, general management of the work. All authors have read and approved the final version of the manuscript and agreed to be accountable for all aspects of the work.

Conflict of interest: the authors declare no apparent or potential conflict of interest related to the publication of this article.

Ethics approval: seven-month-old male mice of two lines, C57Bl (wild type) and 5xFAD (Alzheimer's disease pathology) from the Chernogolovka nursery (Russia) were used in our study. The experiments were conducted in accordance with the protocol for the use of laboratory animals of IEF&B RAS, based on the European Community Directive on the humane treatment of laboratory animals (Directive #86/609 for the Care of Laboratory Animals) and ARRIVE instructions. All applicable international, national, and/or institutional guidelines for the care and use of animals were followed.

Funding: this work was financially supported by the State Order of the I. M. Sechenov Institute of Evolutionary Physiology and Biochemistry, Russian Academy of Sciences (n. 075-00263-25-00).

Acknowledgments: the authors express their deep gratitude to the Center for Collective Use of Scientific Equipment for Physiological, Biochemical and Molecular-Biological Research (CUP) of IEFB RAS.

Received: 8 October 2025.
Accepted: 18 December 2025.

Veterinary Science Development 2025; 9:10639
doi:10.4081/vsd.2025.10639

Abstract

Light and electron microscopy revealed significant neuropathological alterations in both parietal cortical and hippocampal tissues of 7-month-old 5xFAD (familial Alzheimer's disease) transgenic mice, a well-established model of human Alzheimer's disease (AD), compared to age-matched wild-type controls. Key pathological findings included neuronal degeneration, extensive β-amyloid (Aβ) plaque deposition in the neuropil, and astroglial activation with elevated glial fibrillary acidic protein (GFAP) expression in affected brain regions. Consistent with AD-like pathology, 5xFAD mice exhibited cognitive deficits resembling human dementia, which correlated with reduced activity of neprilysin (NEP), the principal amyloid-degrading enzyme. To counteract the reduction in NEP level, we performed daily intraperitoneal administration of the histone deacetylase (HDAC) inhibitor sodium valproate (VA; 200 mg/kg body weight) for one month. VA treatment of adult mice normalized NEP expression levels, restored olfactory and mental functions, and significantly reduced amyloidosis progression. Notably, while VA treatment ameliorated major pathological features, residual ultrastructural abnormalities persisted in cortical and hippocampal tissues. These findings highlight the critical role of amyloid clearance mechanisms in early AD pathogenesis. It can be concluded that the therapeutic potential of NEP upregulation might be crucial as an early therapy strategy applied prior to extensive Aβ plaque formation and irreversible neurodegeneration.

Introduction

Alzheimer's disease (AD) is a chronic, incurable neurodegenerative disorder with significant societal impact, representing the most prevalent cause of age-related cognitive decline.[1-3] The disease is pathologically characterized by senile plaque formation, consisting primarily of aggregated β-amyloid peptide (Aβ). These Aβ aggregates exhibit neurotoxic properties, disrupting synaptic connections and ultimately leading to progressive memory loss, impaired learning capacity and communication abilities, and the inability to perform daily activities.[4,5] Neuroinflammation, particularly through microglial activation, plays an important role in AD pathogenesis. As demonstrated in previous studies, glial activation occurs in response to amyloid accumulation.[6-8] Our earlier investigations of 7-month-old 5xFAD (familial Alzheimer's disease) transgenic mice revealed pathological alterations in the olfactory bulbs, hippocampus, and piriform cortex that are in line with the ultrastructural changes observed in human AD patients.[9-11] Although Aβ accumulation has long been considered irreversible, several amyloid-degrading enzymes have been identified in brain tissue that regulate the aggregation of extracellular Aβ.[12,13] This

discovery highlights the existence of an endogenous neuroprotective system that mitigates the accumulation of neurotoxic Aβ and subsequent neurodegenerative processes.

Mammalian neprilysin (NEP, neutral endopeptidase) has been identified as the principal amyloid-degrading enzyme.[6,13,14] The concentration and activity of NEP in brain regions critically influence amyloid peptide aggregation in AD, with amyloidosis progression demonstrating an inverse correlation with NEP activity levels.[11,15] It was revealed that NEP expression and activity are highest in the striatum and olfactory bulbs, whereas they are substantially lower in cortical and hippocampal regions.[2] Notably, cortical NEP expression undergoes a significant age-dependent decline.[2] Although compounds that modulate NEP expression remain poorly studied, several candidates have been identified that target epigenetic mechanisms mediated by histone deacetylase (HDAC) inhibition.[16,17] Among these, the HDAC inhibitor sodium valproate (VA) has demonstrated efficacy in both *in vitro* and *in vivo* models.[7,18] Mechanistically, VA administration in rodents promotes NEP promoter activation and subsequent upregulation of expression.[18] Our previous work established that chronic VA treatment in 5xFAD transgenic mice both restores cortical NEP mRNA expression to physiological levels and normalizes cognitive function to wild-type performance.[15]

Current evidence indicates that while NEP effectively prevents new amyloid accumulation and aggregation, it lacks the capacity to resolve established senile plaques.[18] Nevertheless, the extent of residual cellular and ultrastructural pathology resulting from pre-existing amyloid deposits prior to HDAC inhibitor therapy remains uncharacterized and warrants experimental investigation. The present study examines how elevated NEP expression affects the structural and ultrastructural organization of the parietal cortex and dorsal hippocampus in 5xFAD transgenic mice relative to wild-type controls.

Materials and Methods

Sample

The study was performed on male mice from two genetic backgrounds: C57Bl/6 (wild-type controls) and 5xFAD (AD model), obtained from the Scientific-Experimental Base "Chernogolovka" (Chernogolovka, Russia). Animals were housed at the Sechenov Institute of Evolutionary Physiology and Biochemistry of the Russian Academy of Sciences (IEPhB RAS; Saint-Petersburg, Russia) under standard conditions (12:12 light-dark cycle, 22±° C, 50-60% humidity) with 4-5 mice per cage and *ad libitum* ac cess to food and water.

The treatment group received sodium VA (Sigma-Aldrich, St. Louis, MO, USA; 200 mg/kg in physiological saline, intraperitoneal [i.p.]) daily for ≥28 days (n=15). Vehicle control received physiological saline (i.p.) (n=15).

Light microscopy

Following deep anesthesia, mice underwent transcardial perfusion with ice-cold 10% neutral-buffered formalin (in 0.1 M phosphate-buffered saline [PBS], pH 7.4). Brains were extracted and post-fixed for 24 hours before processing. Coronal sections, 20 µm thick, containing the parietal cortex and hippocampus (corresponding to 2.0-3.3 mm posterior to bregma, according to Paxinos *et al.*)[19]were cut using a Leica CM1510S cryostat. (Leica Biosystems, Nussloch, Germany). Staining protocols included: Nissl staining with cresyl violet (BioVision, Milan, Italy), or dual cresyl violet/Congo red (4% aqueous; Sigma-Aldrich, St. Louis, MO, USA) for amyloid detection. All sections were analyzed using a Zeiss ImagerA microscope (Carl Zeiss Microscopy GmbH, Jena, Germany) with consistent imaging parameters across groups.

Electron microscopy

For ultrastructural analysis, perfusion fixation employed 1% glutaraldehyde/1% paraformaldehyde in 0.1 M PBS (pH 7.4). Tissue blocks (1 mm^3) from regions of interest were post-fixed in 1% OsO_4, uranyl acetate-contrasted, ethanol-dehydrated, and araldite-embedded as described in Nalivaeva *et al.*[2] Ultrathin sections (50 nm) were cut using a Leica ultramicrotome, mounted on copper grids, and examined with an FEI Tecnai V2 electron microscope at 80 kV (Thermo Fisher Scientific, Oregon, USA).

RNA isolation and quantitative PCR analysis

Total RNA was extracted from dissected brain regions using TRI Reagent® (Molecular Research Center, Inc.) following the manufacturer's protocol. RNA samples (n=12 in each group) were reverse transcribed using Moloney murine leukemia virus (M-MLV) reverse transcriptase to generate cDNA templates for subsequent real-time polymerase chain reaction (PCR) analysis, as previously described.[20]

Primer design

All primers and probes were custom-synthesized by Beagle (St. Petersburg, Russia). The reference gene cyclophilin A (*CycA*) was amplified using the following primer pair:
Forward: 5'-AGGATTCATGTGCCAGGGTG-3'
Reverse: 5'-CTCAGTCTTGGCAGTGCAGA-3'
For NEP quantification, we employed these specific primers:
Forward: 5'-GGATCTTGTAAGCAGCCTCAGC-3'
Reverse: 5'-AGTTGGCACACCGTCTCCAG-3'

Amplification reactions were performed in triplicate using a Bio-Rad C1000 Touch Thermal Cycler equipped with a CFX96 detection system (Bio-Rad, Hercules, CA, USA). Relative mRNA expression levels were calculated using the comparative ΔΔCt method,[21] with normalization to both the housekeeping gene (*CycA*) and control sample values.

Western blot analysis

Parietal cortex (encompassing all cortical layers) and dorsal hippocampus (including CA1, CA3, and dentate gyrus regions) were dissected from wild-type (n=4) and 5xFAD (n=4) mice. Tissues were homogenized in ice-cold 50 mM Tris-HCl buffer (pH 7.4) and centrifuged (2,500×g, 5 min, 4°C). The supernatant was collected, and the pellet was resuspended to confirm the absence of target proteins. Protein concentration was determined using the Bradford assay. Samples containing 25 µg of protein were resolved by 8% sodium dodecyl sulfate-polyacrylamide gel electrophoresis (SDS-PAGE) and then transferred onto polyvinylidene fluoride (PVDF) membranes. Membranes were blocked with 5% non-fat dry milk in PBS containing 0.1% Tween-20 (PBST) for 1 hour at room temperature, followed by overnight incubation at 4°C with primary antibodies: anti-glial fibrillary acidic protein (GFAP; Abcam, #ab6072; 1:1000) and anti-β-actin (Sigma, #A5060; 1:10,000) as a loading control. After washing, membranes were incubated with horseradish peroxidase (HRP)-conjugated secondary antibodies (Abcam anti-rabbit IgG, 1:4000) for 1 hour at room temperature. Protein bands were visualized using Optiblot ECL Ultra Detect Kit (Abcam #ab133409) according to the manufactur-

er's instructions. Band intensities were quantified using ImageLab software (Bio-Rad), with GFAP expression normalized to β-actin levels for each sample.

Statistical analysis

All statistical analyses were performed using GraphPad Prism 9 software. For normally distributed data, we applied parametric statistical methods. Specific analyses included:

i) NEP mRNA expression: one-way analysis of variance (ANOVA) with Fisher's least significant difference (LSD) *post hoc* test for multiple comparisons between wild-type and 5xFAD groups.
ii) Western blot data: non-parametric Mann-Whitney U test for comparisons between 5xFAD and wild-type mice.

Results are presented as mean ± standard error of the mean (SEM). A probability value of $p \leq 0.05$ was considered statistically significant for all analyses.

Results

Light and electron microscopy revealed pathological changes in both cell viability and tissue ultrastructure in the parietal cortex and dorsal hippocampus of 7-month-old 5xFAD mice, compared with age-matched wild-type controls.

Parietal cortex

In contrast to wild-type mice, 5xFAD mice exhibited Aβ aggregates (Congo red-stained senile plaques up to 0.1 mm in diameter) in the parietal cortex. Numerous small plaques were present in the molecular layer, with a higher density in cortical layers II-IV (Figure 1 A,D,E). These spherical formations were typically surrounded by astrocytes and blood vessels. Plaque interiors often contained remnants of degenerating cell bodies and processes. Degenerating neurons were observed in the neuropil near senile plaques in transgenic mice. Some neurons exhibited chromatolysis, characterized by swollen cell bodies and lysis of organelles in the perinuclear cytoplasm. Another degenerative phenotype, hyperchromatosis, was characterized by dark, shrunken cell bodies and dendrites with reduced turgor (Figure 1 F,G). Electron microscopy revealed additional neuropathological alterations in 5xFAD mice (Figure 1 B,C,H,I). Compared to wild-type mice (Figure 1C), transgenic mice exhibited myelin sheath delamination (Figure 1L), axonal atrophy, and neuronal degeneration. Affected neurons showed dilated endoplasmic reticulum channels, vacuolization, and accumulation of disrupted mitochondria with degraded cristae, along with lipofuscin granules and lysosomes. In the parietal cortex, neurodegeneration manifested primarily as chromatolysis, though hyperchromatic and neurofilamentous types were also observed. The latter was marked by cytoplasmic accumulation of neurofilaments (Figure 1I). Additionally, transgenic mice displayed electron-dense, membrane-bound pathological structures in the neuropil and around dying neurons, structures absent in wild-type mice. Figure 1J depicts a pyramidal neuron encircled by these structures, while Figure 1K shows their clusters in the parietal neuropil.

Dorsal hippocampus

Light microscopy of the dorsal hippocampus revealed small senile plaques in both the basal (stratum oriens) and apical (stratum radiatum) layers, as identified by double Nissl and Congo red staining (Figure 2 A,D). In 7-month-old 5xFAD transgenic mice,

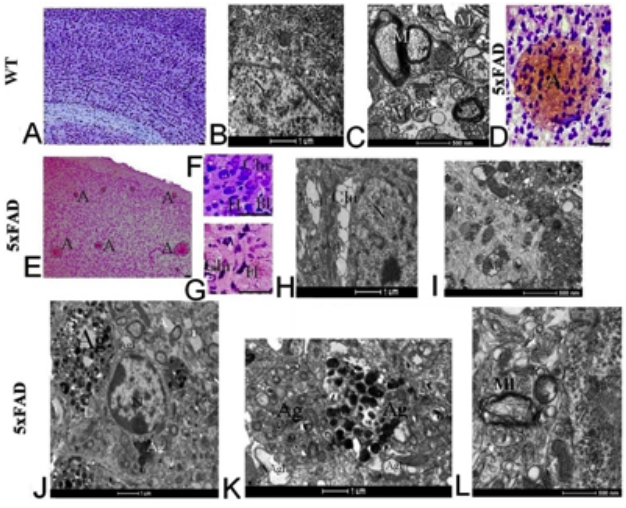

Figure 1. Neurodegenerative changes in the parietal cortex of 7-month-old 5xFAD mice at structural (**A, D-G**) and ultrastructural (**B, C, H-L**) levels. Wild-type mice are shown in panels **A-C**, and 5xFAD transgenic mice in panels **D-L. A**) Parietal cortex section stained with cresyl violet using the Nissl method. **D, E, F, G**) Double staining with Congo red and cresyl violet. Scale bar: 50 µm. FAD, familial Alzheimer's disease; WT, wild-type; Chr, chromatolysis; H, hyperchromatosis; A, senile plaques; Ag, clusters of electron-dense formations; N, neurons; M, mitochondria; Ml, myelin fibers; L, lysosomes; Agl, astroglia processes; Nf, neurofilaments.

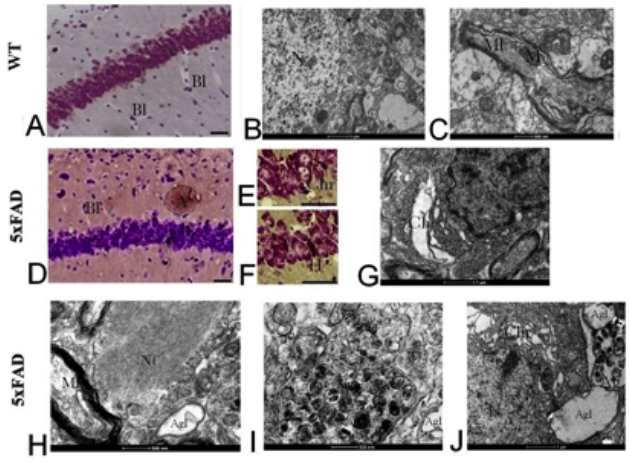

Figure 2. Neurodegenerative changes in the dorsal hippocampus of 5xFAD mice at the structural (**A, D-F**) and ultrastructural (**B, C, G-J**) levels. In wild-type **(A-C**) and 5xFAD transgenic mice **(D-J**) at the age of 7 months. **A**) Section of dorsal hippocampus stained with cresyl violet by the Nissl method. **D-F**) double staining with Congo red and cresyl violet. Scale bar: 50 µm. FAD, familial Alzheimer's disease; WT, wild-type; Chr, chromatolysis; H, hyperchromatosis; Agl, astrocyte processes; A, senile plaques (circled by a dotted line); Ag, accumulations of electron-dense formations; N, neurons; M, mitochondria; Ml, myelin fibers; Nf, neurofilaments; Bl, blood vessels.

these plaques were often surrounded by blood vessels and numerous astrocytes. Neuronal degeneration in these mice manifested as two primary phenotypes. Chromatolytic degeneration was characterized by cellular edema, organelle lysis, and cytoplasmic swelling (Figure 2 B,C,E,F). Hyperchromatosis was marked by dark, shrunken cell bodies and degenerated dendritic processes (Figure 2G). In the dorsal hippocampus of 5xFAD mice, hyperchromatosis was the predominant degenerative phenotype, contrasting with the parietal cortex, where chromatolysis was more common. Additionally, a neurofilamentous degeneration type was observed, with dense neurofilament accumulations in neuronal cell bodies and processes (Figure 2H). Ultrastructural analysis further revealed several pathological features in transgenic mice that were absent in wild-type controls. Frequent clusters of electron-dense structures were observed (Figure 2 I,J), along with myelin sheath delamination in hippocampal fibers (Figure 2H). Plaques showed a distribution bias, being more prevalent in the stratum oriens and stratum radiatum than in the stratum pyramidale, and were more abundant in the neuropil than adjacent to neuronal somata. Degenerating neurons and electron-dense structures were consistently surrounded by astrocytic processes, suggesting active glial involvement in the pathological response.

Effect of sodium valproate on the structure of the parietal cortex and dorsal hippocampus of 5xFAD mice

The observed structural alterations in the nervous tissue of the cortex and hippocampus in 5xFAD mice correlate with cerebral Aβ accumulation, potentially attributable to reduced activity of amyloid-degrading enzymes, particularly NEP.[2] We detected decreased NEP expression levels in these animals (Figure 3 A,C). To address this deficiency, we employed pharmacological treatment using the HDAC inhibitor VA (200 mg/kg body weight, administered daily for one month). This treatment successfully restored NEP expression to normal levels, demonstrating its potential for correcting neurodegenerative pathology in both the parietal cortex and hippocampus of transgenic mice. One month following VA administration to 5xFAD transgenic mice, we conducted electron microscopic analysis of parietal cortical and hippocampal tissues. Despite treatment, persistent neuropathological features were observed, including degenerating neuronal remnants in both cortex (Figure 4) and hippocampus (Figure 5), senile plaques and electron-dense aggregates (Figures 4 B,C and 5C). Regional-specific distribution patterns were also observed. Cortical electron-dense structures are preferentially localized near neuronal soma. Hippocampal aggregates predominantly occupied the neuropil of the stratum oriens and stratum radiatum. Notably, we identified some electron-dense structures in cortical intercellular spaces (Figure 4D) that were absent in hippocampal tissue. Both regions exhibited pronounced astrogliosis, with numerous astrocytes and their processes surrounding degenerating neurons (Figures 4A and 5B).

Light microscopic analysis using Nissl and Congo red double

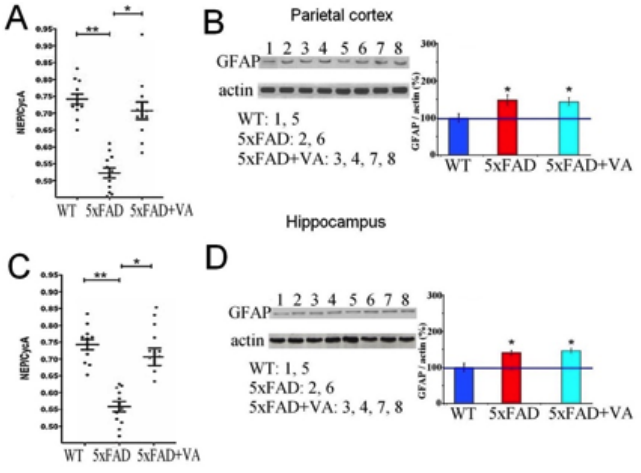

Figure 3. A, C) Relative content of NEP mRNA in the parietal cortex (**A**) and dorsal hippocampus (**C**) of wild-type mice, 5xFAD mice (*p<0.05, **p<0.01, Mann-Whitney U test), and 5xFAD mice treated with VA. Data are presented as mean ± error of the mean. **B, D**) Analysis of the astrocytic marker GFAP in the parietal cortex (**B**) and dorsal hippocampus (**D**) of wild-type and transgenic 5xFAD mice (5xFAD and 5xFAD+VA). Left panels show representative immunochemical staining after electrophoresis; right panels show quantitative analysis of GFAP levels. *p<0.05 indicates a statistically significant difference between 5xFAD and wild-type mice (Mann-Whitney U test; n=2-4 per group). Data are presented as mean ± error of the mean and expressed as % of control (wild-type set to 100%).

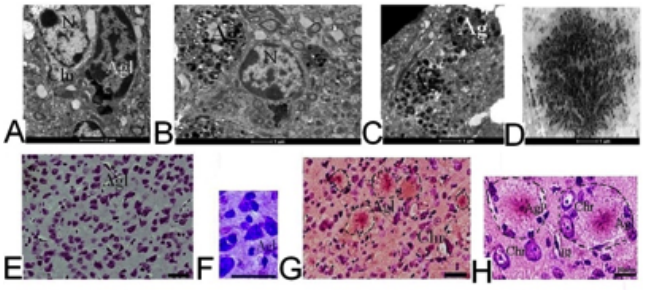

Figure 4. Effect of VA on the structural (**E-H**) and ultrastructural (**A-D**) organization of the parietal cortex tissue in 5xFAD mice. **A-D**) electron microscopy; **G, H**) double staining with Congo red and cresyl violet. Scale bar: 50 μm. **D**) Pathological formation in the intercellular space of the parietal cortex tissue. Senile plaques are outlined by a dotted line; Agl, astrocyte processes; Chr, neurons in a state of chromatolysis; Ag, clusters of electron-dense formations; N, neurons; Bl, blood vessels.

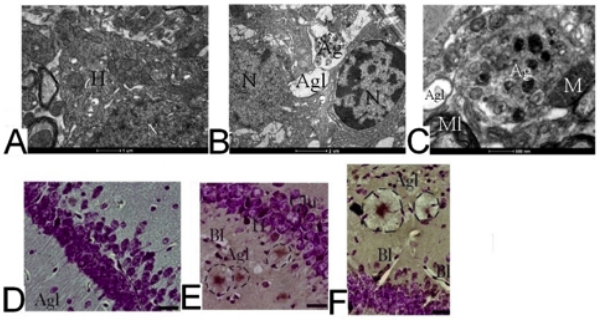

Figure 5. Effect of VA on the structural (**D-F**) and ultrastructural (**A-C**) organization of the dorsal hippocampal tissue of 5xFAD mice. **A-C**) electron microscopy; **E, F**) double staining with Congo red and cresyl violet. Scale bar: 50 μm. Senile plaques are outlined by a dotted line; Agl, astrocytes; Chr, neurons in a state of chromatolysis; H, neuronal hyperchromatosis; Ag, clusters of electron-dense formations; N, neurons; Bl, blood vessels.

staining revealed some alterations in astrocytic glia within the parietal cortex and dorsal hippocampus of 5xFAD transgenic mice compared to wild-type controls (Figures 4 and 5). Reactive astrocytes were predominantly localized near blood vessels and degenerating neurons, frequently surrounding membrane-bound clusters of electron-dense pathological formations in both perineuronal and neuropil regions (Figures 4 B,C and 5C). Quantitative analysis of GFAP content demonstrated marked astroglial activation in transgenic animals. The parietal cortex showed 50.2% higher GFAP expres-sion than wild-type mice (U=17.1, p=0.02, Mann-Whitney U-test). The dorsal hippocampus showed an even greater increase in GFAP levels (146.9% *vs.* wild-type; U=17.1, p=0.02), suggesting that astroglial responses in the hippocampus are more pronounced than in the cortex. VA treatment did not significantly alter GFAP levels in either region (Figure 3 B,D). These results indicate that 5xFAD mice develop robust astrogliosis in both regions, and that VA administration does not affect GFAP content despite its reported neuroprotective effects.

Discussion

AD represents a major global health challenge, characterized by progressive memory loss, spatial disorientation, and severe neurodegeneration in elderly populations.[1,3] To advance therapeutic development, researchers developed the 5xFAD transgenic mouse model (C57BL/6 strain; hemizygous Tg(APPSwFlLon, PSEN1M146L L286V)6799Vas/J), which carries mutations in both the *APP* and *PSEN1* genes.[22-24] This model faithfully recapitulates key pathological features of human AD, including progressive neurodegenerative changes in neural tissue, development of cognitive dysfunction, and characteristic Aβ deposition patterns[23] Our previous behavioral studies,[9-11] supported by existing literature, demonstrate significant differences between 5xFAD and wild-type mice in both cognitive and olfactory functions. Notably, these animals develop both measurable cognitive impairments as well as olfactory dysfunction between 4-6 months of age, coinciding with widespread Aβ deposition and progressive neuroinflammatory processes.[23] To elucidate the mechanisms underlying behavioral impairments, our previous studies conducted comparative analyses of nervous tissue in the olfactory bulbs and piriform cortex of 7-month-old 5xFAD transgenic mice *vs.* wild-type controls.[9-11] These investigations revealed neurodegenerative pathology characterized by senile plaques and degenerating neuronal cells. Our light and electron microscopic analysis of the parietal cortex and dorsal hippocampus in 7-month-old 5xFAD mice revealed neurodegenerative features, including neuronal degeneration manifesting as chromatolysis, hyperchromatosis, and neurofilamentous degeneration, membrane-bound clusters of electron-dense pathological aggregates in the neuropil, and numerous senile plaques in both cellular and fibrous layers. At the ultrastructural level, we observed accumulations of electron-dense pathological structures surrounded by membranes in the neuropil of both brain regions. In the literature, similar formations were previously reported in different brain areas of 5xFAD mice.[9,10] These structures are clearly pathological and likely associated with amyloidosis progression, as they are absent in wild-type mice and rats. While the precise nature of these formations remains incompletely understood, similar structures have been documented in 5xFAD mice by other researchers, described as dystrophic axons.[25,26] Several studies have demonstrated activated astroglial and microglial cells phagocytosing such aggregates.[8,27]

We also detected abundant senile plaques in both the cellular and fibrous layers of the parietal cortex and hippocampus. The accumulation of amyloid in brain tissue may result from deficient levels and activity of NEP, the primary enzyme involved in neurotransmitter and amyloid degradation. Notably, NEP expression and activity are highest in the striatum and olfactory bulbs, while cortical and hippocampal levels are substantially lower and decline with age.[11,15] The Aβ peptide of humans consists of two distinct domains: an N-terminal hydrophilic fragment (residues 1-16) and a C-terminal hydrophobic fragment (residues 17-42). The hydrophobic fragment forms the aggregate core through hydrogen bonding and hydrophobic interactions, while the hydrophilic fragment faces outward. The metal-binding N-terminal fragment (1-16) plays a crucial role in plaque formation through chelation of transition metals (zinc, iron, and copper) by histidine residues His6, His13, and His14.[28] Additional modifications in the hydrophilic domain, such as racemization of aspartic acid residues (Asp7 and Asp23), further promote amyloid aggregation.[29] In wild-type rodents (mice and rats), Aβ lacks aggregation propensity due to sequence differences from human Aβ. Specifically, the rat Aβ sequence contains three substitutions: Gly5 replaces Arg5, Phe10 replaces Tyr10, and Arg13 replaces His13.[29] These substitutions significantly alter the peptide's physicochemical properties, preventing aggregation. Current evidence indicates that NEP primarily prevents additional amyloid accumulation and aggregation but cannot eliminate pre-existing senile plaques.[2,12] Therefore, the extent of residual pathological changes caused by amyloid accumulation prior to treatment with HDAC inhibitors requires thorough investigation. Our investigation shows the preliminary description of brain tissue structure in adult 5xFAD mice after treatment by VA during the period of developing amyloidosis and neurodegeneration. We conducted experiments on the effects of multiple injections of the HDAC inhibitor VA in these transgenic mice. VA treatment in 5xFAD mice altered the state of astrocytes and their processes in the parietal cortex and dorsal hippocampus. According to the literature, astrocytic activation is triggered by amyloid accumulation.[7]

Previously, we showed that long-term administration of VA to 5xFAD mice restores NEP mRNA expression and behavioral characteristics of animals to values observed in wild-type mice.[15] The transgenic mice demonstrated improved olfactory function and restored cognitive abilities.[15]

Neuroinflammation and microglial activation contribute significantly to disease pathogenesis.[6,7,30] In 5xFAD mice, we observed hypertrophy of astrocytic cell bodies, significant swelling, and enlargement of astrocytic processes following VA administration. These morphological changes were evident in both the parietal cortex and dorsal hippocampus. The observed astrocytic process activation, coupled with increased GFAP expression, suggests ongoing neuroinflammatory processes in these brain regions of 5xFAD mice. Our findings align with established literature documenting astroglial activation and microglial phagocytosis of degenerating neural elements.[8,27]

VA administration produced several beneficial effects, including normalization of NEP expression levels, attenuation of neurodegenerative processes, modulation of astroglial activation state (known to be triggered by amyloid accumulation),[27] and correction of behavioral impairments.[1,15]

Conclusions

Our combined morphological and behavioral findings in the 5xFAD transgenic model provide valuable insights that may advance understanding of AD pathology in humans and suggest the importance of early therapy. These results demonstrate that modulating the amyloid clearance system, particularly through upregulation of NEP expression in brain tissue, may be an effective early therapeutic strategy to prevent the onset of amyloidosis and irreversible structural damage in the cortex and hippocampus.

References

1. Revi M. Alzheimer's Disease. Therapeutic Approaches. Adv Exp Med Biol 2020;1195:105-16.
2. Nalivaeva NN, Zhuravin IA, Turner AJ. Neprilysin expression and functions in development, ageing and disease. Mech Ageing Dev 2020;192:111363.
3. Thakral S, Yadav A, Singh V, et al. Alzheimer's disease: Molecular aspects and treatment opportunities using herbal drugs. Ageing Res Rev 2023;88:101960.
4. Ballard C, Gauthier S, Corbett A, et al. Alzheimer's disease. Lancet 2011;377:1019-31.
5. Scheltens P, De Strooper B, Kivipelto M, et al. Alzheimer's disease. Lancet 2021;397:157-90.
6. Al-Ghraiybah NF, Wang J, Alkhalifa AE, et al. Glial Cell-Mediated Neuroinflammation in Alzheimer's Disease. Int J Mol Sci 2022;23:10572.
7. Arendt T. Synaptic plasticity and cell cycle activation in neurons are alternative effector pathways: the Dr. Jekyll and Mr. Hyde concept of Alzheimer's disease or the yin and yang of neuroplasticity. Prog Neurobiol 2003;71:83-248.
8. Sos KE, Mayer MI, Takács VT, et al. Amyloid β induces interneuron-specific changes in the hippocampus of APPNL-F mice. PLoS One 2020;15:e0233700.
9. Tumanova NL, Vasiliev DS, Dubrovskaya NM, Nalivaeva NN. Morphofunctional changes in the brain nervous tissue of 5xFAD transgenic mice. Cell Tissue Biol 2022;16:380-91.
10. Tumanova NL, Vasilev DS, Dubrovskaya NM, Nalivaeva NN. Neurodegenerative changes in the structural and ultrastructural organization in the pyriform cortex of 5xFAD transgenic mice. J Evol Biochem Physiol 2022;58:1225-39.
11. Vasilev DS, Dubrovskaya NM, Tumanova NL, Nalivaeva NN. Analysis of expression of the amyloid-degrading enzyme neprilysin in brain structures of 5xFAD transgenic mice. J Evol Biochem Physiol 2022;58:193-203.
12. Baranello RJ, Bharani KL, Padmaraju V, et al. Amyloid-beta protein clearance and degradation (ABCD) pathways and their role in Alzheimer's disease. Curr Alzheimer Res 2015;12:32-46.
13. Carson JA, Turner AJ. Beta-amyloid catabolism: roles for neprilysin (NEP) and other metallopeptidases? J Neurochem 2002;81:1-8.
14. Turner AJ. Exploring the structure and function of zinc metallopeptidases: old enzymes and new discoveries. Biochem Soc Trans 2003;31:723-7.
15. Vasilev DS, Dubrovskaya NM, Tumanova NL, et al. Valproate administration to adult 5xFAD mice upregulates expression of neprilysin and improves olfaction and memory. J Mol Neurosci 2024;74:110.
16. Klein C, Mathis C, Leva G, et al. Gamma-Hydroxybutyrate (Xyrem) ameliorates clinical symptoms and neuropathology in a mouse model of Alzheimer's disease. Neurobiol Aging 2015;36:832-44.
17. Wang Z, Zhang XJ, Li T, et al. Valproic acid reduces neuritic plaque formation and improves learning deficits in APP(Swe) /PS1(A246E) transgenic mice via preventing the prenatal hypoxia-induced down-regulation of neprilysin. CNS Neurosci Ther 2014;20:209-17.
18. Nalivaeva NN, Belyaev ND, Turner AJ. Sodium valproate: an old drug with new roles. Trends Pharmacol Sci 2009;30:509-14.
19. Paxinos G, Franklin KBJ. The mouse brain in stereotaxic coordinates. 2nd Edition, Academic Press, San Diego; 2001.
20. Malkin SL, Amakhin DV, Veniaminova EA, et al. Changes of AMPA receptor properties in the neocortex and hippocampus following pilocarpine-induced status epilepticus in rats. Neuroscience 2016;327:146-55.
21. Livak KJ, Schmittgen TD. Analysis of relative gene expression data using real-time quantitative PCR and the 2−ΔΔCT method. Methods 2001;25:402-8.
22. Kosel F, Hamilton JS, Harrison SL, et al. Reduced social investigation and increased injurious behavior in transgenic 5xFAD mice. J Neurosci Res 2021;99:209-22.
23. Pádua MS, Guil-Guerrero JL, Lopes PA. Behaviour hallmarks in Alzheimer's disease 5xFAD mouse model. Int J Mol Sci 2024;25:6766.
24. Richard B C, Kurdakova A, Baches S, et al. Gene Dosage Dependent Aggravation of the Neurological Phenotype in the 5XFAD Mouse Model of Alzheimer's Disease. J Alzheimers Dis 2015;45:1223-36.
25. Kosik KS. The neuritic dystrophy of Alzheimer's disease: degeneration or regeneration? In: Hefti F, Brachet P, Will B, Christen Y (eds.) Growth factors in Alzheimer's disease. Berlin, Heidelberg: Springer; 1991, pp. 234-40.
26. Li Q, Weiland A, Chen X, et al. Ultrastructural characteristics of neuronal death and white matter injury in mouse brain tissues after intracerebral hemorrhage: coexistence of ferroptosis, autophagy, and necrosis. Front Neurol 2018;9:581.
27. Gomez-Arboledas A, Davila JC, Sanchez-Mejias E, et al. Phagocytic clearance of presynaptic dystrophies by reactive astrocytes in Alzheimer's disease. Glia 2018;66:637-53.
28. Sugiki T, Utsunomiya-Tate N. Site-specific aspartic acid isomerization regulates self-assembly and neurotoxicity of amyloid-β. Biochem Biophys Res Commun 2013;441:493-8.
29. Kulikova AA, Makarov AA, Kozin SA. The role of zinc ions and structural polymorphism of β-amyloid in the initiation of Alzheimer's disease. Mol Biol 2015;49:249-63.
30. Wang C, Zong S, Cui X, et al. The effects of microglia-associated neuroinflammation on Alzheimer's disease. Front Immunol 2023;14:1117172.